doi:10.1038/nature07247

LETTERS

Three-dimensional optical metamaterial with a negative refractive index

Jason Valentine[1]*, Shuang Zhang[1]*, Thomas Zentgraf[1]*, Erick Ulin-Avila[1], Dentcho A. Genov[1], Guy Bartal[1] & Xiang Zhang[1,2]

Metamaterials are artificially engineered structures that have properties, such as a negative refractive index[1–4], not attainable with naturally occurring materials. Negative-index metamaterials (NIMs) were first demonstrated for microwave frequencies[5,6], but it has been challenging to design NIMs for optical frequencies and they have so far been limited to optically thin samples because of significant fabrication challenges and strong energy dissipation in metals[7,8]. Such thin structures are analogous to a monolayer of atoms, making it difficult to assign bulk properties such as the index of refraction. Negative refraction of surface plasmons was recently demonstrated but was confined to a two-dimensional waveguide[9]. Three-dimensional (3D) optical metamaterials have come into focus recently, including the realization of negative refraction by using layered semiconductor metamaterials and a 3D magnetic metamaterial in the infrared frequencies; however, neither of these had a negative index of refraction[10,11]. Here we report a 3D optical metamaterial having negative refractive index with a very high figure of merit of 3.5 (that is, low loss). This metamaterial is made of cascaded 'fishnet' structures, with a negative index existing over a broad spectral range. Moreover, it can readily be probed from free space, making it functional for optical devices. We construct a prism made of this optical NIM to demonstrate negative refractive index at optical frequencies, resulting unambiguously from the negative phase evolution of the wave propagating inside the metamaterial. Bulk optical metamaterials open up prospects for studies of 3D optical effects and applications associated with NIMs and zero-index materials such as reversed Doppler effect, superlenses, optical tunnelling devices[12,13], compact resonators and highly directional sources[14].

NIMs, first described by Veselago more than 40 years ago[1] and recently discussed in the framework of metamaterials[2], arise from the fact that both the permittivity and the permeability of the materials are simultaneously negative. In the past several years, much effort has been dedicated to the engineering and extension of the functionalities of metamaterials at terahertz[15–17] and optical frequencies[7,8,10,18–21]. Metal–dielectric–metal fishnet structures were among the earliest demonstrations of optical NIMs. These structures, however, consist of a single functional layer along the direction of propagation. This is equivalent to an atomic monolayer, making it difficult to explore phenomena in three dimensions and develop device applications. Moreover, as a result of their resonant nature, these systems suffer substantial loss at optical frequencies. On the basis of the above, it is therefore imperative to realize low-loss bulk optical NIMs if we are to demonstrate unambiguously the unique effects associated with negative index of refraction.

Recently, it has been suggested theoretically that stacking up multiple fishnet functional layers along the propagation direction constitutes a promising approach for achieving a 3D optical NIM[22] (Fig. 1a). This cascading leads to a strong magneto-inductive coupling between neighbouring functional layers[23]. As demonstrated recently[24], the tight coupling between adjacent *LC* resonators through mutual inductance results in a broadband negative index of refraction with low loss, which is similar to the material response of left-handed transmission lines[25,26]. In addition, the loss is further reduced owing to the destructive interference of the antisymmetric currents across the metal film, effectively cancelling out the current flow in the centre of the film[23].

Here we experimentally demonstrate the first 3D optical NIM by directly measuring the angle of refraction from a prism made of cascaded fishnet metamaterial. The experimental results, along with numerical calculations, serve as direct evidence of zero and negative phase index in the metamaterial.

The 3D fishnet metamaterial is fabricated on a multilayer metal-dielectric stack by using focused ion-beam milling (FIB), which is capable of cutting nanometre-sized features with a high aspect ratio. Figure 1b shows the scanning electron microscopy (SEM) image of the proposed 3D fishnet pattern, which was milled on 21 alternating films of silver and magnesium fluoride, resulting in ten functional layers.

To measure the index of refraction of the 3D metamaterial experimentally, a prism was created in the multilayer stack (Fig. 2a, b). Measurements of the refractive index of these structures were performed by observing the refraction angle of light passing through the prism by Snell's law. This provides a direct and unambiguous deter-

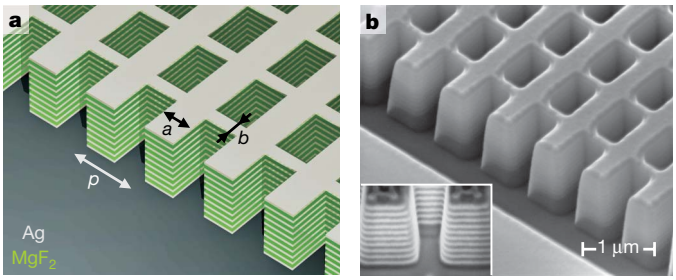

Figure 1 | Diagram and SEM image of fabricated fishnet structure. **a**, Diagram of the 21-layer fishnet structure with a unit cell of $p = 860$ nm, $a = 565$ nm and $b = 265$ nm. **b**, SEM image of the 21-layer fishnet structure with the side etched, showing the cross-section. The structure consists of alternating layers of 30 nm silver (Ag) and 50 nm magnesium fluoride (MgF_2), and the dimensions of the structure correspond to the diagram in **a**. The inset shows a cross-section of the pattern taken at a 45° angle. The sidewall angle is 4.3° and was found to have a minor effect on the transmittance curve according to simulation.

[1]NSF Nano-scale Science and Engineering Center (NSEC), 3112 Etcheverry Hall, University of California, Berkeley, California 94720, USA. [2]Material Sciences Division, Lawrence Berkeley National Laboratory, Berkeley, California 94720, USA.
*These authors contributed equally to this work.

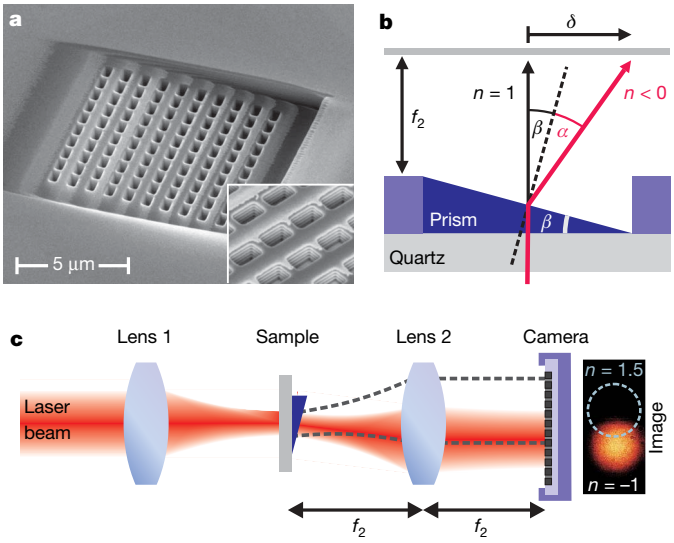

Figure 2 | SEM image of NIM prism and schematics of experimental setup. **a**, SEM image of the fabricated 3D fishnet NIM prism. The unit cell size is identical to that shown in Fig. 1a. The inset shows a magnified view with the film layers visible in each hole. **b**, Geometry diagram of the angle measurement; δ corresponds to the position difference of the beam passing through a window in the multilayer structure ($n = 1$) and prism sample. By measuring δ, the absolute angle of refraction α can be obtained. **c**, Experimental setup for the beam refraction measurement. The focal length of lens 1 is 50 mm and that of lens 2 is $f_2 = 40$ mm. Lens 2 is placed in a $2f$ configuration, resulting in the Fourier image at the camera position.

mination of the refractive index, because the refraction angle depends solely on the phase gradient that the light beam experiences when refracted from the angled output face. We used a femtosecond synchronously pumped optical parametric oscillator as a tunable light source to determine the refractive index at different wavelengths. The beam was focused on the sample, and a charge-coupled device (CCD) camera was placed in the Fourier plane (Fig. 2c).

Figure 3a shows the beam shift δ resulting from the bending of light at the prism output at different wavelengths, ranging from 1,200 to 1,700 nm. The measurement was performed on a prism of angle $\beta = 5.0^\circ$ and the beam shift is plotted along with reference measurements of transmission through a window, without the presence of the prism (left panel). Clearly, as the wavelength increases, the beam shift resulting from the prism refraction is changing from positive to negative, indicating a transition from a positive index in the shorter wavelengths to a negative index in the longer wavelengths. At a wavelength λ of 1,475 nm, the index of refraction is approaching zero; that is, the beam does not acquire any phase while propagating in the metamaterial. Consequently there is no phase gradient at the angled output face and the exiting beam is exactly normal to the output face (see dashed lines in Figs 2b and 3a).

Figure 3b depicts the measured refractive index of the 3D fishnet metamaterial at various wavelengths. The refractive index varies from $n = 0.63 \pm 0.05$ at 1,200 nm to $n = -1.23 \pm 0.34$ at 1,775 nm. The refractive index was determined from multiple measurements of two fishnet prisms with angles of $\beta = 5.0^\circ$ and 4.7° and for wavelengths ranging from 1,200 to 1,800 nm. Although there is a correlation between the beam spot positions shown in Fig. 3a and the refractive index in Fig. 3b, it should be noted that Fig. 3b shows the average of measurements on different prisms with the standard deviation as error bars, whereas Fig. 3a shows an individual measurement. The experimental results are found to be in good agreement with the theoretical predictions (black line in Fig. 3b) on the basis of rigorous coupled-wave analysis (RCWA). The measured negative refraction angle is a direct result of negative phase evolution for light propagating inside the sample caused by a negative refractive index. This is illustrated in Fig. 3c by a numerical calculation of the in-plane electromagnetic field distribution in the fishnet prism at

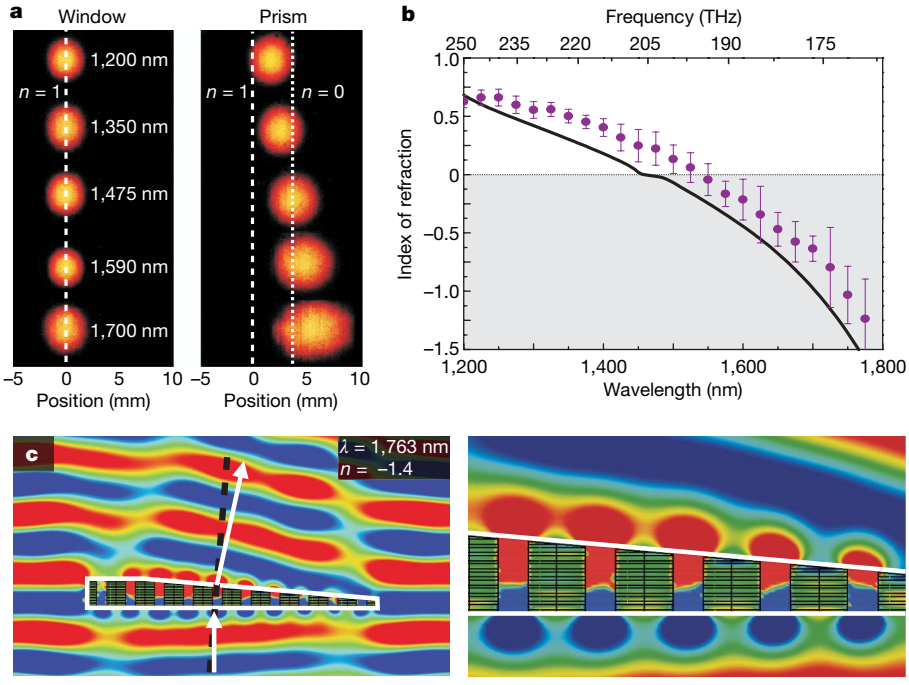

Figure 3 | Experimental results and finite-difference time-domain simulations. **a**, Fourier-plane images of the beam for the window and prism sample for various wavelengths. The horizontal axis corresponds to the beam shift δ, and positions of $n = 1$ and $n = 0$ are denoted by the white lines. The image intensity for each wavelength has been normalized for clarity. **b**, Measurements and simulation of the fishnet refractive index. The circles show the results of the experimental measurement with error bars (s.d., $n = 4$ measurements). The measurement agrees closely with the simulated refractive index using the RCWA method (black line). **c**, Left: simulation of the in-plane electric field component for the prism structure at 1,763 nm, showing the phase front of the light. Negative-phase propagation resulting from the negative refractive index leads to negative refraction angle as measured by the beam shift in the experiment. Right: magnified plot of the field distribution in the prism.

$\lambda = 1{,}763$ nm, where the structure shows a refractive index of $n = -1.4$. A movie of the evolution of the electric field generated with commercial finite-difference time-domain software at the same wavelength is also presented in Supplementary Information. Because of the negative phase propagation inside the metamaterial, the electromagnetic wave emerging from the thicker part of the prism experiences phase advance compared with that passing through the thinner parts, causing the light to bend in the negative direction at the exit interface. We note that the refractive index remains consistent for the fishnet metamaterial with three or more functional layers along the propagation direction, which leads to a uniform wavefront exiting from the prism (see Supplementary Information).

To acquire a clear understanding of the 3D metamaterial's optical response, we separate the fishnet into two subsets and calculate the dispersion curves with RCWA. The first constituent is a 3D array of metal wires aligned with the polarization direction of the incident electric field (Fig. 4a). This array serves as an effective medium with lowered volumetric plasma frequency (220 THz), below which wave propagation is not allowed because of negative effective permittivity[27]. The second constituent is a 3D array of metal strips along the direction of the magnetic field (Fig. 4b), in which induced antisymmetric conductive currents across the dielectric layers give rise to a magnetic bandgap between 135 and 210 THz. This is further confirmed by the plots of the magnetic fields at two frequencies, below and above the bandgap. Above the bandgap the magnetic response is positive, as shown in Fig. 4d, where the magnetic field component between the strips is in phase with the external field. Above the bandgap, the metal strips have a moderately negative response, as shown in Fig. 4e, where the magnetic field between the strips is out of phase. Finally, these two structures are merged to form the 3D fishnet metamaterial, for which the dispersion relation is shown in Fig. 4c. A propagation band with negative slope appears in the overlapped region of the forbidden gaps of both electric and magnetic media, demonstrating that the negative-index behaviour in the 3D cascaded fishnet does indeed result from the fact that both the electric permittivity and the magnetic permeability are negative.

In addition, transmittance measurements were performed on the 3D fishnet metamaterial made of 21 layers with the use of a Fourier-transform infrared microscope (Nicolet Nic-Plan IR microscope). Figure 4f shows the measured transmittance spectrum along with the numerically calculated transmittance. The simulation predicts a broad negative-index band spanning from 1.45 μm to 2.2 μm (shaded region), which coincides with the high transmission band from 1.5 μm to 1.8 μm. As mentioned previously, this wide band of negative index results from the strong coupling between neighbouring layers. The measured transmittance has similar features to those of the calculation, namely two peaks imposed over the transmission band that are slightly red-shifted with respect to the numerical results. These features are due to the Fabry–Pérot effect, in which the impedance mismatch leads to reflectance at the metamaterial/air and metamaterial/glass interfaces. Although the peaks are visible at lower refractive index values owing to the lower loss, the Fabry–Pérot effect cannot be clearly seen in the transmission spectra for larger negative index at longer wavelength where the loss is higher, resulting in broadening and extinction of spectral features. We note that the transmittance in the negative-index band is one-quarter of the numerically calculated value, which is probably due to imperfections in the fabrication. Nevertheless, our simulations show that the presence of loss in the coupled fishnet metamaterial has a minimal impact on the dispersion relation (see Supplementary Information). This is because the 3D fishnet structure operates far from the band edge (Fig. 4c), where resonance is not significant. This explains the good agreement between the experimentally measured and simulated refractive indices despite the fabrication imperfections.

Finally, we estimate the figure of merit (FOM $= -\mathrm{Re}(n)/|\mathrm{Im}(n)|$) of our fishnet multilayer structure. The material loss (that is, $\mathrm{Im}(n)$) is conservatively estimated from the measured transmittance and reflectance data of the 21-layer sample, assuming a single pass of light through the metamaterial, as $\mathrm{Im}(n) = (\lambda/4\pi d)\ln[(1-R)/T]$, where λ, d, R and T are the wavelength, sample thickness, reflectance and transmittance, respectively. The dispersion of the simulated

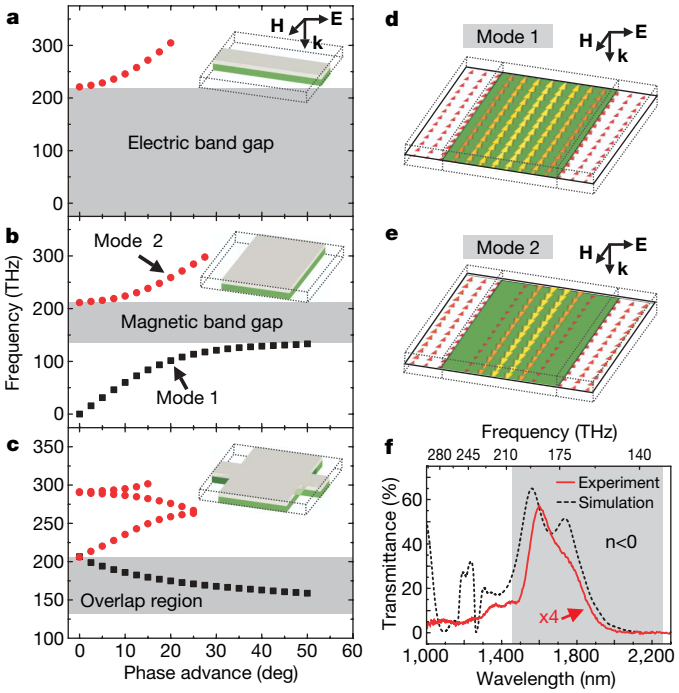

Figure 4 | Dispersion relations, field plots and transmission for the 3D fishnet structure. In all plots the grey area corresponds to the negative-index region as determined by simulations. **a**, Dispersion relation for a 3D array of metal wires aligned along the electric field **E**, where **k** denotes the incident propagation vector. The dotted lines in the diagram mark the unit cell size, which is identical in **a**–**e**, and correspond to Fig. 1a. **b**, Dispersion relation of a 3D array of metal strips along the magnetic field **H**. **c**, The dispersion for the 3D fishnet structure. A dispersion curve with negative slope appears within the overlapped region of the electric bandgap and magnetic bandgap if both structures are combined. **d**, Magnetic field plot below the bandgap. **e**, Magnetic field plot above the bandgap. **f**, Experimental transmittance curve (red line) of a 22×22 unit cell fishnet structure ($17.6 \times 17.6\ \mu m^2$ total patterned area), which has been multiplied by four for clarity. The simulated transmittance (black dotted line) was obtained with RCWA.

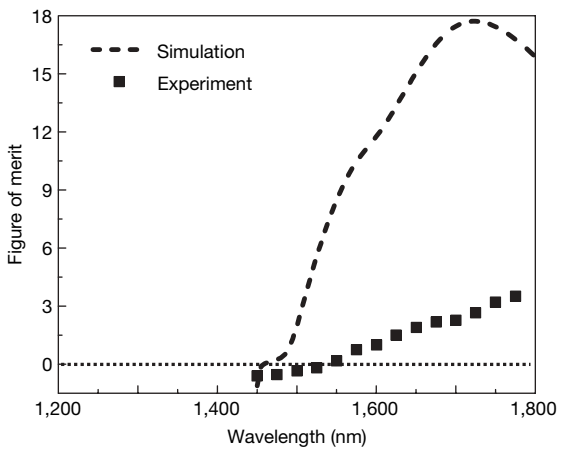

Figure 5 | Figure of merit for the 3D fishnet structure. Plot of FOM against wavelength for the simulation (dashed line) and experiment (squares). The lower experimental FOM is due to reduced transmission resulting from fabrication imperfections. The experimental FOM reaches 3.5 at 1,775 nm, where $\mathrm{Re}(n) = -1.23$.

and experimental FOM is plotted in Fig. 5. The FOM is 3.5 at $\lambda = 1{,}775$ nm (where $\mathrm{Re}(n) = -1.23$), which is among the highest experimental values so far recorded at optical frequencies[19]. For ideal fabrication conditions, the FOM could rise as high as about 20, as determined from theoretical calculations. We emphasize that our results are different from recent reports of negative refraction[11,28] in anisotropic media with hyperbolic dispersion (equivalent to negative 'group index') but positive phase velocity.

The fishnet metamaterial has a period about $\lambda/20$ in the vertical direction. The propagation of light travelling along this direction or within some angular range is dominated by this deep sub-wavelength period and not by the in-plane period, as long as the wavevector projection on the in-plane directions is small compared with the in-plane reciprocal lattice vector of the fishnet metamaterial. There is only a single propagating mode in the negative-index frequency region, justifying the description of the fishnet metamaterial with an effective index. In contrast, if higher dielectric materials such as silicon ($n \approx 3.6$) are used to serve as the dielectric layer, the ratio between the wavelength and in-plane period can be significantly increased because of the larger capacitance in the *LC* circuit.

Unlike the negative index obtained from photonic crystals[29], the negative index presented here results from simultaneous negative magnetic and electric responses and shows a resemblance to the left-handed transmission line due to the tight coupling between the adjacent *LC* resonators. The negative index occurs in the first propagation band and with smooth negative-phase evolution along the light propagation direction, which differs from the negative refraction obtained in photonic crystals.

Here we have experimentally demonstrated the first 3D NIM at optical frequencies and directly measured the refractive index of a NIM prism in the free space. The 3D optical metamaterials may offer the possibility to explore a large variety of optical phenomena associated with zero and negative refractive index, as well as applications in the scaling down of photonics and imaging.

METHODS SUMMARY

In the numerical studies of the 3D fishnet metamaterial, the intrinsic losses of the metal are included[30]. The multilayer stack was deposited by electron-beam evaporation of alternating layers of silver (30 nm) and magnesium fluoride (50 nm) resulting in a total thickness of 830 nm. Two different configurations of the fishnet samples were fabricated on the multilayer stack. Samples of the first configuration consist of 22×22 in-plane fishnet unit cells and were used for the characterization of the transmittance. The second configuration (prism sample) was formed by etching the film at an angle β to the film surface, using FIB. The exact angle was measured with an atomic force microscope and was found to vary slightly between samples. A 10×10 fishnet pattern was subsequently milled in the prism.

To obtain the absolute angle of refraction, a window with an area equal to that of the prism was etched through the multilayer stack to serve as a reference. The window and prism Fourier images were measured for all wavelengths on an indium gallium arsenide infrared camera and the total beam shift δ of the spot centre was calculated. Consequently, the angle of refraction α at the surface of the prism is given as $\alpha = \beta - \arctan(\delta/f_2)$. Snell's law ($n = \sin\alpha/\sin\beta$) was used to calculate the real part of the refractive index of the sample. The imaginary part of the refractive index of the sample was obtained from transmittance and reflectance data acquired with a 21-layer sample of the first configuration (as described above).

Full Methods and any associated references are available in the online version of the paper at www.nature.com/nature.

Received 20 March; accepted 11 July 2008.
Published online 11 August 2008.

1. Veselago, V. G. The electrodynamics of substances with simultaneously negative values of ε and μ. *Sov. Phys. Usp.* **10,** 509–514 (1968).
2. Smith, D. R., Pendry, J. B. & Wiltshire, M. C. K. Metamaterials and negative refractive index. *Science* **305,** 788–792 (2004).
3. Pendry, J. B. Negative refraction makes a perfect lens. *Phys. Rev. Lett.* **85,** 3966–3969 (2000).
4. Tsakmakidis, K. L., Boardman, A. D. & Hess, O. 'Trapped rainbow' storage of light in metamaterials. *Nature* **450,** 397–401 (2007).
5. Shelby, R. A., Smith, D. R. & Schultz, S. Experimental verification of a negative index of refraction. *Science* **292,** 77–79 (2001).
6. Parazzoli, C. G., Greegor, K., Li, K., Koltenbah, B. E. C. & Tanielian, M. Experimental verification of negative index of refraction using Snell's law. *Phys. Rev. Lett.* **90,** 107401 (2003).
7. Panoiu, N. C. & Osgood, R. M. Numerical investigations of negative refractive index metamaterials at infrared and optical frequencies. *Opt. Commun.* **223,** 331–337 (2003).
8. Shalaev, V. M. *et al.* Optical negative-index metamaterials. *Nature Photonics* **1,** 41–48 (2007).
9. Lezec, H. J., Dionne, N. A. & Atwater, H. A. Negative refraction at visible frequencies. *Science* **316,** 430–432 (2007).
10. Liu, N. *et al.* Three-dimensional photonic metamaterials at optical frequencies. *Nature Mater.* **7,** 31–37 (2008).
11. Hoffman, A. J. *et al.* Negative refraction in semiconductor metamaterials. *Nature Mater.* **6,** 946–950 (2007).
12. Silveirinha, M. & Engheta, N. Tunneling of electromagnetic energy through subwavelength channels and bends using epsilon-near-zero materials. *Phys. Rev. Lett.* **97,** 157403 (2006).
13. Edwards, B. *et al.* Experimental verification of epsilon-near-zero metamaterial coupling and energy squeezing using a microwave waveguide. *Phys. Rev. Lett.* **100,** 033903 (2008).
14. Enoch, S. *et al.* A metamaterial for directive emission. *Phys. Rev. Lett.* **89,** 213902 (2002).
15. Yen, T. J. *et al.* Terahertz magnetic response from artificial materials. *Science* **303,** 1494–1496 (2004).
16. Padilla, W. J. *et al.* Dynamical electric and magnetic metamaterial response at terahertz frequencies. *Phys. Rev. Lett.* **96,** 107401 (2006).
17. Chen, H. T. *et al.* Active terahertz metamaterial devices. *Nature* **444,** 597–600 (2006).
18. Linden, S. *et al.* Magnetic response of metamaterials at 100 terahertz. *Science* **306,** 1351–1353 (2004).
19. Soukoulis, C. M., Linden, S. & Wegener, M. Negative refractive index at optical frequencies. *Science* **315,** 47–49 (2007).
20. Dolling, G., Wegener, M. & Linden, S. Realization of a three-functional-layer negative-index photonic metamaterial. *Opt. Lett.* **32,** 551–553 (2007).
21. Alu, A. & Engheta, N. Three-dimensional nanotransmission lines at optical frequencies: A recipe for broad band negative-refraction optical metamaterials. *Phys. Rev. B* **75,** 024304 (2007).
22. Zhang, S. *et al.* Optical negative-index bulk metamaterials consisting of 2D perforated metal-dielectric stacks. *Opt. Express* **14,** 6778–6787 (2006).
23. Li, T. *et al.* Coupling effect of magnetic polariton in perforated metal/dielectric layered metamaterials and its influence on negative refraction transmission. *Opt. Express* **14,** 11155–11163 (2006).
24. Eleftheriades, G. V. Analysis of bandwidth and loss in negative-refractive-index transmission-line (NRI–TL) media using coupled resonators. *IEEE Microw. Wireless Components Lett.* **17,** 412–414 (2007).
25. Grbic, A. & Eleftheriades, G. V. Overcoming the diffraction limit with a planar left-handed transmission-line lens. *Phys. Rev. Lett.* **92,** 117403 (2004).
26. Lai, A., Carloz, C. & Itoh, T. Composite right-/left-handed composite transmission line metamaterials. *IEEE Microw. Mag.* **5,** 34–50 (2004).
27. Pendry, J. B., Holdenz, A. J., Robbins, D. J. & Stewartz, W. J. Low frequency plasmons in thin-wire structures. *J. Phys. Condens. Matter* **10,** 4785–4809 (1998).
28. Fan, X. B. *et al.* All-angle broadband negative refraction of metal waveguide arrays in the visible range: Theoretical analysis and numerical demonstration. *Phys. Rev. Lett.* **97,** 073901 (2006).
29. Notomi, M. Theory of light propagation in strongly modulated photonic crystals: Refraction-like behavior in the vicinity of the photonic band gap. *Phys. Rev. B* **62,** 10696 (2000).
30. Johnson, P. B. & Christy, R. W. Optical constants of the noble metals. *Phys. Rev. B* **6,** 4370–4379 (1972).

Supplementary Information is linked to the online version of the paper at www.nature.com/nature.

Acknowledgements We acknowledge funding support from US Army Research Office (ARO) MURI programme 50432-PH-MUR and partly by the NSF Nano-scale Science and Engineering Center DMI-0327077. We thank H. Bechtel and M. C. Martin for assisting in measurements of near-infrared transmission and reflection, and S. R. J. Brueck for discussion. T.Z. acknowledges a fellowship from the Alexander von Humboldt Foundation. Multilayer deposition was performed at the Molecular Foundry, Lawrence Berkeley National Laboratory, which is supported by the Office of Science, Office of Basic Energy Sciences, of the US Department of Energy under contract no. DE-AC02-05CH11231.

Author Information Reprints and permissions information is available at www.nature.com/reprints. Correspondence and requests for materials should be addressed to X.Z. (xiang@berkeley.edu).

METHODS

In the numerical studies of the 3D fishnet metamaterial, with the exception of Figs 3c and 4d, e, we used a RCWA, which expands the electromagnetic field into 13×13 diffraction orders and matches the boundary conditions at each interface. Specifically, the numerical refractive index in Fig. 3b, the dispersion curves in Fig. 4a–c and the numerical figure of merit in Fig. 5 were calculated using a modal analysis given in ref. 22. Figures 3c and 4d, e were calculated with commercial finite-difference time-domain software (CST Microwave Studio). In the simulations, a Drude model was used for the dielectric parameters of silver, with plasma frequency $\omega_p = 9.0$ eV and scattering frequency $\gamma = 0.054$ eV. The scattering frequency is increased by a factor of three compared to that of the bulk silver[30] in order to account for the additional loss of surface scattering.

In the experimental setup (Fig. 2c), light from the optical parametric oscillator (Spectra-Physics) was focused onto the prism with an achromatic lens (lens 1); the second lens (lens 2) was placed at its focal position. The position of the beam at the focal distance of lens 2 (f_2) was used to calculate the angle of refraction. As a result of limited camera imaging area, only the zero-order Fourier image was recorded. To obtain the absolute angle of refraction, a window with an area equal to that of the prism was etched through the multilayer stack to serve as a reference. The window's Fourier image was measured at all wavelengths, giving a reference position corresponding to a refractive index of 1. The centres of the beam spot for both the window and prism samples were determined by fitting the intensity with a 2D Gaussian profile and the total beam shift (δ) at the position of the camera was calculated by taking the difference between the beam spot centres.